A Novel Self-Consistent Model Based Optimal Filter Design for the Improved Dynamic Performance of 3-phase PLLs for Phase Tracking Under Grid Imperfections

Sambhav R Jain, Pradhyumna Ravikirthi & Nagamani Chilakapati

Journal of Control, Automation and Electrical Systems
formerly CONTROLE & AUTOMAÇÃO

ISSN 2195-3880
Volume 25
Number 5

J Control Autom Electr Syst (2014)
25:608-619
DOI 10.1007/s40313-014-0137-3

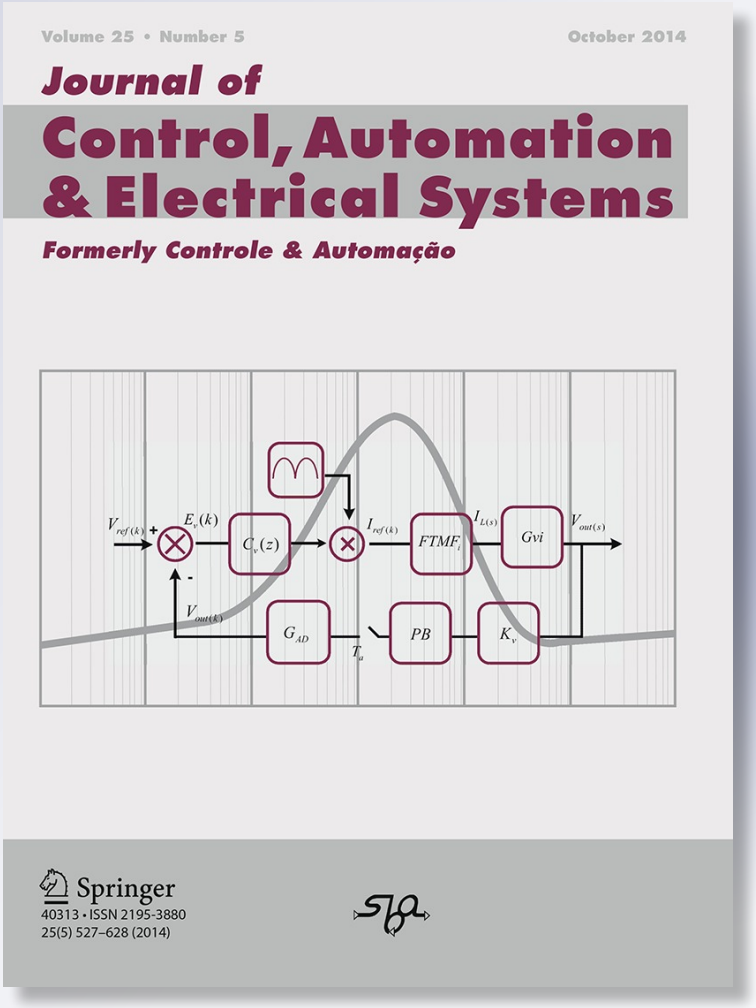

Springer

J Control Autom Electr Syst (2014) 25:608–619
DOI 10.1007/s40313-014-0137-3

A Novel Self-Consistent Model Based Optimal Filter Design for the Improved Dynamic Performance of 3-phase PLLs for Phase Tracking Under Grid Imperfections

Part 1: Theory and Mathematical Basis

Sambhav R Jain · Pradhyumna Ravikirthi · Nagamani Chilakapati

Received: 21 October 2013 / Revised: 20 May 2014 / Accepted: 24 May 2014 / Published online: 25 June 2014

Abstract In the context of recent advancements in 3-phase phase-locked loop (PLL) structures to tackle grid imperfections, this paper attempts to shift focus towards dynamic response optimization for fast tracking of disturbed grids, as opposed to Wiener optimization, a *trade-off* between filtering characteristic and dynamic response. In this respect, an ingenious self-consistent model (SCM)-based approach is proposed which explores filter design in the presence of frequency shifts and phase jumps, and facilitates the analytical computation of *unique* loop filter parameters. Trial and error in filter parameter selection is inconvenient, but more importantly, even rigorous trials would be insufficient in qualifying the non-existence of a better design. Having eliminated trial and error, this novel technique limits transients to user specifications while fixing on an optimum damping ratio, to yield the best fit. The design methodology is applied to three existing 3-phase PLL structures modelled in MATLAB/Simulink, and the proposed method is further evaluated through extensive simulations and performance comparisons with the traditional Wiener approach. To enhance the understanding of model behaviour and the feasibility of practical implementation, comprehensive three-dimensional (3-D) lookup tables are presented. They enable the study of optimized filter parameter variations for a range of grid disturbances, and broaden the application to filter optimization in real-time. In the interest of the reader, this paper is structurally split into two parts. Part 1 covers the premise and theory that explicates the proposed SCM methodology. The detailed analysis and verification of the SCM are covered in Part 2.

Keywords Self-consistent model · Loop filter design · 3-D lookup tables · Dynamic performance · Wiener optimization · Grid imperfections

S. R. Jain (✉) · P. Ravikirthi · N. Chilakapati
Department of Electrical and Electronics Engineering,
National Institute of Technology, Tiruchirappalli 620015, India
e-mail: sambhav.eee@gmail.com

P. Ravikirthi
e-mail: pradhyumnarao@gmail.com

N. Chilakapati
e-mail: cnmani@nitt.edu

Present address
S. R. Jain
Texas Instruments (India) Pvt. Ltd., Bagmane Tech Park,
C V Raman Nagar, Bangalore 560093, India

1 Introduction

Modern power system network is highly interconnected for optimal use of the available resources, such as thermal, hydro and nuclear, to serve the industrial and domestic loads located near or far. For the purpose of providing a reliable and controllable supply to the consumers, flexible AC transmission controllers (FACTS), which are essentially power electronic controllers, are also incorporated in strategic locations of the network. Further, the network includes distributed generation (DG) units based on local, renewable energy sources such as wind, solar, geothermal, etc. In this scenario, continuous, accurate and dynamic synchronization of the power electronic controllers with the complex network is of utmost importance for the smooth and stable operation of the overall system. The synchronous reference frame (SRF) PLL (Kaura and Blasko 1997; Chung 2000) was one of the important milestones in phase tracking for grid synchronization, which stimulated further developments in this field.

In the past two decades, non-linear loads have caused power quality degradation of electrical distribution systems by injecting characteristic harmonics. In general, grid proliferation is seen in the form of harmonics, voltage unbalance,

phase jumps and frequency deviations (Weidenbrug et al. 1993; Bollen 1996; Gulez 2008). The SRF PLL is very sensitive to voltage unbalance and harmonic distortion (Karimi-Ghartemani and Iravani 2004; da Silva et al. 2010), under which the amplitude of the output voltage vector has unsettled higher order oscillations, with a nominal bandwidth setting. Moreover, although a reduction in the bandwidth of the PI feedback loop helps in cancelling the effect of harmonics, the same also contributes to a poorer dynamic response. Thus, with the conventional SRF PLL, a trade-off needs to be made between filtering and fast tracking, under distorted utility conditions.

Over the years, the literature has seen the SRF PLL evolving into larger, mathematically intuitive schemes (Kesler and Ozdemir 2011; González-Espín et al. 2012; Rodríguez et al. 2005, 2006, 2007; Liccardo et al. 2011; Guo et al. 2011; Wang et al. 2013), either targeting power quality improvement in a distorted utility/load condition (Kesler and Ozdemir 2011; González-Espín et al. 2012), or striving to filter unwanted components of the utility voltage and extract the positive sequence fundamental component for phase tracking. For instance, Rodríguez et al. (2006) proposed a dual second-order generalized integrator (DSOGI)-based PLL using two quadrature signal generators (SOGI-QSG) and a positive sequence calculator (PSC) before the final SRF stage. The positive sequence component is fed to the SRF block to make the DSOGI PLL frequency adaptive. The decoupled double synchronous reference frame (DDSRF) PLL (Rodríguez et al. 2007) deals with voltage unbalance by applying two separate Park transformations on reference frames rotating in the opposite direction. An intuitive decoupling network splits the positive and negative sequence components in the synchronous reference frame and the positive sequence component is utilized by the ensuing SRF stage for frequency and phase tracking. Guo et al. (2011) suggested the use of multiple, polarity-selective complex coefficient filters (MCCFs) to reject negative sequence components and eliminate higher order harmonics in the input. Even here, the final stage is an SRF PLL, with the overall scheme being frequency adaptive.

The way in which these schemes have attacked the filtering limitation of SRF PLL is unique. However, for the design of PI filter parameters, each of the above used the Wiener optimization method (Gardner 2005). The crux of Wiener method is to choose a nominal value of damping ratio δ (say $1/\sqrt{2}$), and calculate the natural frequency ω_n based on the input signal power, deviation in frequency and noise spectral density. However, since it is difficult to obtain the stochastic information of noise, an empirical trade-off is used, where ω_n is determined by trial and error. DSOGI PLL uses this empirical trade-off on Wiener method (Chung 2000). In DDSRF PLL, the proportional gain k_p and the integral gain k_i of the final SRF stage are chosen using this method. MCCF PLL also adheres to this method in fixing δ (as $1/\sqrt{2}$), and adjusting ω_n for better harmonic rejection and fast response time.

The poor dynamic response of these improvised SRF-based PLLs is attributed to the PI-based control (da Silva et al. 2010; Liccardo et al. 2011; Lee et al. 2014). The fact that the Wiener method was mostly used in choosing the PI parameters may well be a factor affecting the dynamic response in such cases. The need for better tuning of the PI filter parameters is also highlighted in Golestan et al. (2012); Kulkarni and John (2013). Moreover, very limited literature is available on the assumption-free design of the filter parameters of an SRF-based 3-phase PLL on the basis of transient response to phase jumps and frequency shifts.

In Sect. 2, we question the appropriateness of Wiener method in today's context, and bring in a strong need to adopt an approach that focusses emphatically on the dynamic response optimization, in the specific case of improvised SRF-based 3-phase PLLs. Under this premise, a novel self-consistent model (SCM)-based optimization technique is proposed, which (i) decouples the inverse dependency between filtering and fast tracking, thus eliminating the need for trade-off, (ii) replaces cumbersome trial and error in filter parameter selection by a direct analytical approach, (iii) extracts the most optimum PI filter gains to meet the user-specified error limits under a worst-case combination of frequency excursion and phase jump. The two algorithms that form the SCM framework, *viz.*, error quantization and damping optimization, are presented in Sect. 3, where we propose to solve them self-consistently.

As can be anticipated, this design methodology is solely aimed at optimally improving the dynamic response of SRF-based 3-phase PLLs, leaving the task of filtering to the augmented stages prior to SRF PLL. It will soon be clear that while the SCM is a filter tuning technique for one class of PLLs, the ability to deal with various grid imperfections is primarily dependent on the PLL topology itself.

2 Premise

2.1 Linear SRF PLL Model

Conventional SRF PLL uses two transformations on the 3-phase grid voltage, namely the Clarke transformation and the Park transformation. The convention followed for reference frame transformation (Krause et al. 2002) is established in Fig. 1, where v_β and v_α represent the voltage components in the stationary reference frame, while ${v_q}^e$ and ${v_d}^e$ represent those in the synchronous reference frame.

In the case of a balanced grid, the Clarke and Park transformed voltages are given by

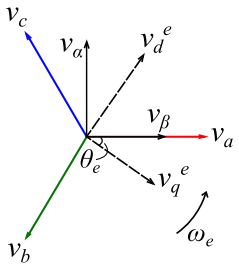

Fig. 1 Stationary and synchronous reference frame components

$$\begin{bmatrix} v_\beta \\ v_\alpha \end{bmatrix} = \begin{bmatrix} V_m \cos\theta_{ef} \\ -V_m \sin\theta_{ef} \end{bmatrix} \tag{1}$$

$$\begin{bmatrix} {v_q}^e \\ {v_d}^e \end{bmatrix} = \begin{bmatrix} V_m \cos(\theta_{ef} - \hat{\theta}) \\ -V_m \sin(\theta_{ef} - \hat{\theta}) \end{bmatrix} \tag{2}$$

respectively, where V_m is the peak magnitude, θ_{ef} is the phase angle of the grid phase voltage and $\hat{\theta}$ is the estimated phase angle tracked by the SRF PLL, seen in Fig. 2.

When the estimated angle closely follows the grid phase angle, the d-component of the transformed voltage in Eq. (2) can be expressed as the error component. i.e.

$${v_d}^e = -V_m \sin(\theta_{ef} - \hat{\theta}) \approx -V_m(\theta_{ef} - \hat{\theta}). \tag{3}$$

The approximation in Eq. (3) holds true as long as the PLL is in its lock-range, and is of much significance because it allows us to obtain a linearised model of the SRF PLL, which in turn enables the design and optimization of the PI loop filter, to achieve desired performance. Analogizing Eq. (3) with the linear model obtained in Fig. 3, we find $E_m = -V_m$ and $\theta = \theta_{ef}$ in the case of a balanced grid.

For a grid affected with unbalance, however, the error component is given by

$${v_d}^e = -{V_m}^{+1} \sin(\theta_{ef} - \hat{\theta}) - {V_m}^{-1} \sin(-\theta_{ef} - \hat{\theta}) \tag{4}$$

and the same linear model in Fig. 3 holds true with E_m and θ as per Table 1, where

$$\mathrm{K}_{-1} = \frac{{V_m}^{-1}}{{V_m}^{+1}} \tag{5}$$

and ${V_m}^{+1}$ and ${V_m}^{-1}$ are the positive and negative sequence components of the unbalanced grid, respectively. It is noted that the zero sequence current can flow only when (i) the neutral is grounded, and (ii) a fourth wire wye is used (Blackburn 1993). Considering a 3-phase 3-wire system, the zero sequence components are thus omitted.

Similarly, for a grid affected with harmonics, the error component is given by

$$\begin{aligned} {v_d}^e = &- {V_m}^{+1} \sin(\theta_{ef} - \hat{\theta}) - {V_m}^{+5} \sin(-5\theta_{ef} - \hat{\theta}) \\ &- {V_m}^{+7} \sin(7\theta_{ef} - \hat{\theta}) - {V_m}^{+11} \sin(-11\theta_{ef} - \hat{\theta}) \\ &- {V_m}^{+13} \sin(13\theta_{ef} - \hat{\theta}) - \cdots \end{aligned} \tag{6}$$

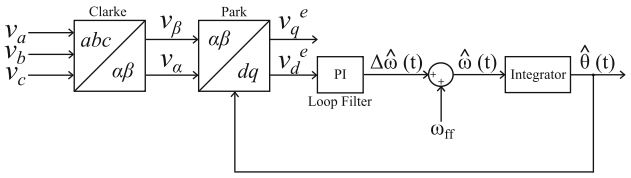

Fig. 2 Conventional SRF PLL

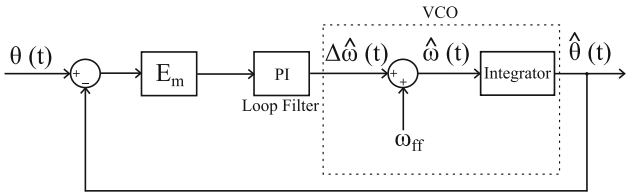

Fig. 3 Linear model of SRF PLL in time domain

Table 1 Linear model parameters for different grid imperfections

Case	E_m	θ (input)
Balanced grid	$-V_m$	θ_{ef}
Unbalanced grid	$-{V_m}^{+1}$	$\theta_{ef} - \mathrm{K}_{-1}\sin(2\theta_{ef})$
Harmonics in the grid	$-{V_m}^{+1}$	$\theta_{ef} - \mathrm{K}_{+6}\sin(6\theta_{ef})$ $- \mathrm{K}_{+12}\sin(12\theta_{ef}) - \cdots$

and the model in Fig. 3 holds good with E_m and θ as per Table 1, where

$$\mathrm{K}_{+n} = \frac{{V_m}^{+(n-1)} - {V_m}^{+(n+1)}}{{V_m}^{+1}} \tag{7}$$

and n represents the order of harmonic.

It is clear from Table 1 that the input to the SRF PLL is free of oscillations in the case of a clean grid, and has higher order oscillations if the grid is unbalanced or affected by harmonics.

2.2 The Two Design Aspects of a PLL

2.2.1 Filtering Characteristic

The first design aspect of a closed loop PLL is its filtering characteristic. Filtering response primarily depends on the bandwidth of a closed loop system. Although there is no unique definition of bandwidth, natural frequency (ω_n) and loop gain ($2\delta\omega_n$) are often used to describe bandwidth in this context. Moreover, according to Gardner (2005), amongst natural frequency and loop gain, the latter is a better measure of bandwidth.

To understand the relation between bandwidth and filtering response, consider the s-domain equivalent of the linear SRF PLL model, as shown in Fig. 4.

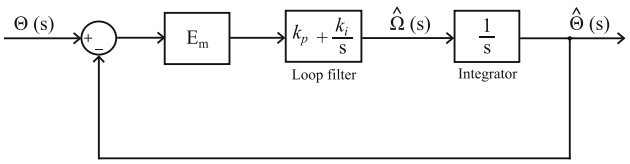

Fig. 4 Linear s-domain model of SRF PLL

The closed loop transfer function of this system is of the form

$$H_c(s) = \frac{\hat{\Theta}(s)}{\Theta(s)} = \frac{2\delta\omega_n s + {\omega_n}^2}{s^2 + 2\delta\omega_n s + {\omega_n}^2} \tag{8}$$

where

$$\omega_n = \sqrt{E_m k_i} \tag{9}$$

$$\delta = \frac{E_m k_p}{2\omega_n}. \tag{10}$$

By Bode magnitude theory, when a sinusoidal input of certain amplitude and frequency is fed to this system, the input amplitude should see itself getting multiplied at the output by a factor M, given by

$$M = |H_c(j\omega)| = \sqrt{\frac{{\omega_n}^4 + 4\delta^2{\omega_n}^2\omega^2}{\left({\omega_n}^2 - \omega^2\right)^2 + 4\delta^2{\omega_n}^2\omega^2}}. \tag{11}$$

For input frequencies much greater than the natural frequency ($\omega \gg \omega_n$), as in Table 1, the multiplication factor (rather called the attenuation factor) reduces to

$$M = \frac{2\delta\omega_n}{\omega}. \tag{12}$$

From Eq. (12), it is clear that the higher the input frequencies are, the more is the attenuation. But it is also visible that the higher the bandwidth ($2\delta\omega_n$) is, the lesser is the attenuation for the same range of frequencies and the poorer is the filtering characteristic of the system. Thus, it is established that bandwidth and filtering response of this closed loop system have an inverse relationship.

2.2.2 Dynamic Performance

The second crucial design aspect of a PLL is its dynamic performance. When the grid voltage experiences a sudden change in frequency, it is required that a PLL be able to track this change with minimum transients. The transient response of a PLL is primarily described by its settling time (t_0).

To derive a relationship between bandwidth and settling time, consider the system subjected to a step change in frequency. Figure 5 shows the phase error variation with time, for a case of $\delta < 1$, governed by the equation

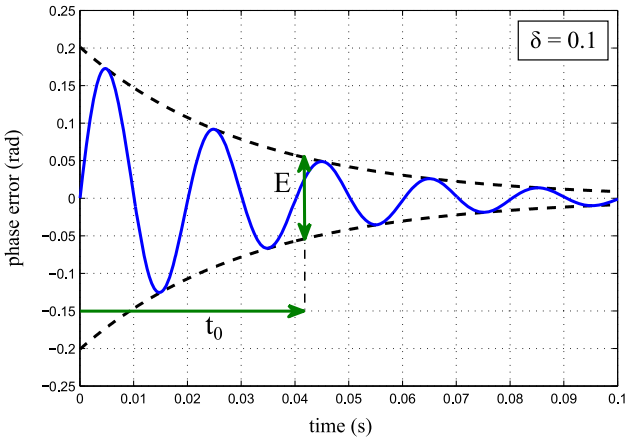

Fig. 5 Phase error as a function of time, with the error envelope marked

$$e(t) = \frac{e^{-\delta\omega_n t}}{\omega_d}\Delta\omega_{\text{step}}\sin(\omega_d t) \tag{13}$$

where ω_d is the damped natural frequency, given by

$$\omega_d = \omega_n\sqrt{1-\delta^2}, \tag{14}$$

and $\Delta\omega_{\text{step}}$ is the step change in frequency, given by

$$\Delta\omega_{\text{step}} = \omega - \omega_{\text{ff}}. \tag{15}$$

ω_{ff} is the centre frequency of the voltage controlled oscillator (VCO, Fig. 3), or the output frequency of the VCO when the input voltage fed to it is zero.

The error band E at settling time t_0 can be computed from Eq. (13), and is given by

$$E = \frac{2\,\Delta\omega_{\text{step}}}{\omega_n\sqrt{1-\delta^2}}\,e^{-\delta\omega_n t_0}. \tag{16}$$

The normalized error E_N, or the error per unit frequency step can be expressed as

$$E_N = \frac{E}{\Delta\omega_{\text{step}}} = \frac{2\,e^{-\delta\omega_n t_0}}{\omega_n\sqrt{1-\delta^2}}. \tag{17}$$

From Eq. (17), it is deduced that the higher the bandwidth ($2\delta\omega_n$) is, the lower is the settling time t_0 for a given error band specification, thus establishing an inverse relationship between bandwidth and settling time of this system.

2.3 Decoupling of 'Filtering Versus Fast Tracking'

It is shown that increasing the bandwidth improves the dynamic response while affecting filtering adversely, and vice versa. Hence, though it is required that both bandwidth and settling time be in control of the designer, filtering and

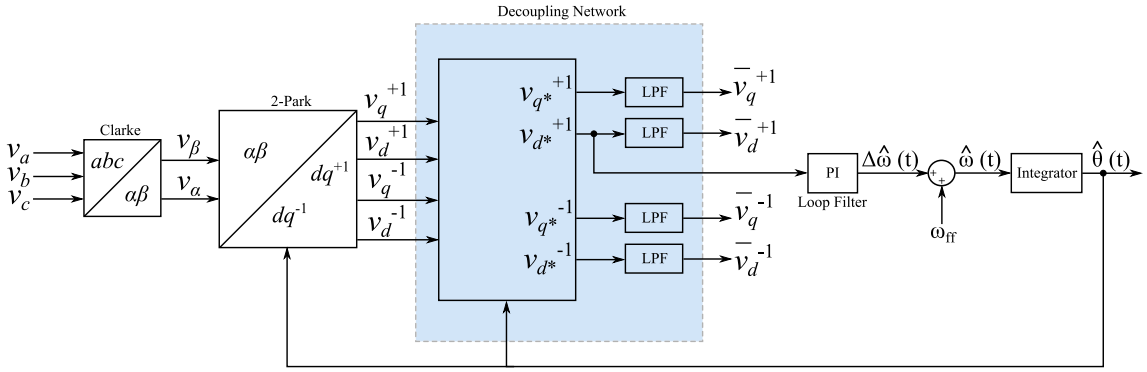

Fig. 6 DDSRF stage augmented to the SRF PLL

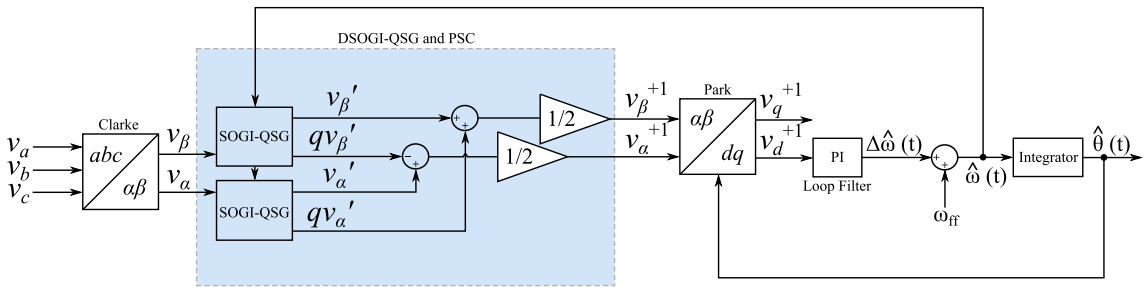

Fig. 7 DSOGI stage augmented to the SRF PLL

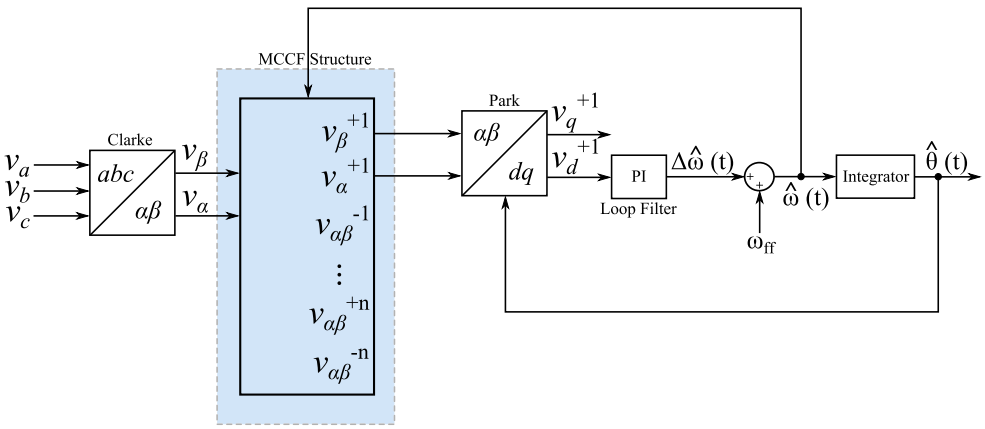

Fig. 8 MCCF stage augmented to the SRF PLL

fast tracking are an inconsistency, and the final design is usually expected to be a trade-off between the two, which leads us to Wiener optimization, as discussed previously.

At this juncture, it is crucial to note that the Wiener method was devised in a time when the 3-phase PLL structure was only capable of tracking a grid devoid of unbalance and harmonics. Inherently, the Wiener method is aimed at achieving a good trade-off between filtering and fast dynamic response. The use of this method was justified in the past, considering minimal grid proliferation then. But with the recent developments in 3-phase PLL structures (Rodríguez et al. 2006, 2007; Guo et al. 2011), filtering is taken care of by the various stages augmented to the SRF block, as highlighted in Figs. 6, 7, and 8. These augmented stages sift the unwanted oscillations injected by grid imperfections, and feed a filtered input to the final SRF stage. Hence, in designing the loop filter of the final SRF PLL stage, emphasis should be given to the dynamic response, as opposed to using a trade-off like in Wiener method. This would enable faster recovery (lock-in) from a grid situation (like frequency step and/or phase jump), without allowing instability to creep in.

Section 3 introduces the development of the SCM, which enables filter design of the final SRF stage by taking advantage of this decoupling, and provides an analytical solution

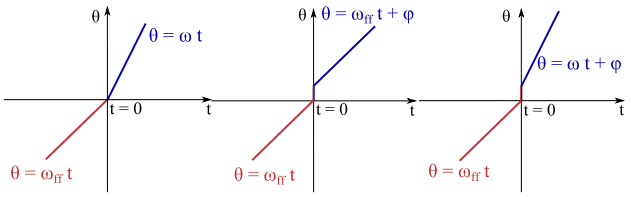

(a) Frequency shift **(b)** Phase jump **(c)** Combined effect

Fig. 9 Inputs to SRF PLL

to arrive at unique filter parameters without any trial and error like in the Wiener method. As discussed, this technique focusses on improving the PLL transient response to frequency and phase fluctuations in the grid, and in doing so, extracts the most optimum PI filter gains to contain error within the user-specified limits.

3 SCM-Based Filter Design

The need to have SRF PLL as the last stage in 3-phase PLLs like DDSRF, DSOGI, MCCF, etc. is justified by its innate ability to track frequency shifts and phase jumps. Hence in designing the SRF PLL for better dynamics, it is necessary to understand its transient response to the phenomena of frequency shift and phase jump.

3.1 Effect of Frequency Shift and Phase Jump

Consider the input of SRF PLL to be in the form of

$$\theta(t) = \omega t + \phi. \tag{18}$$

At time $t = 0$, consider a frequency shift from ω_{ff} to ω and a phase jump from 0 to ϕ in the input, as depicted by Fig. 9. Analysis of the system response thus comprises studying the effect of a ramping input along with a step offset. Using Laplace transform, the response of SRF PLL for the case of $\delta < 1$[1] can be derived, and the phase tracking error $[\theta(t) - \hat{\theta}(t)]$ can thus be obtained as

$$e(t) = \frac{e^{-\delta\omega_n t}}{\omega_d}\Big[(\omega-\omega_{\text{ff}})\sin(\omega_d t)-\phi\,\omega_n \sin(\omega_d t-\gamma)\Big] \tag{19}$$

where γ is the damping angle as in

$$\gamma = \cos^{-1}\delta. \tag{20}$$

In Eq. (19), $\omega - \omega_{\text{ff}}$ denotes the step change in frequency ($\Delta\omega_{\text{step}}$) and ϕ denotes the phase jump, considering $\phi_{t=0^-} = 0$. The envelope which contains this error can be deduced as

$$\pm\left[\frac{e^{-\delta\omega_n t}}{\omega_d}\sqrt{{\Delta\omega_{\text{step}}}^2 + \phi^2{\omega_n}^2 - 2\Delta\omega_{\text{step}}\phi\omega_n\delta}\right].$$

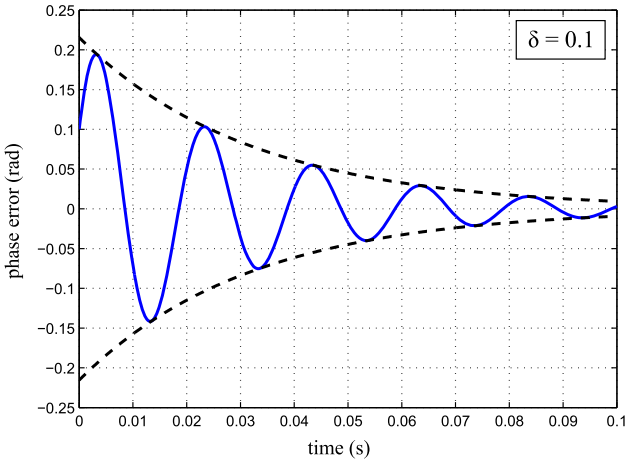

Fig. 10 Error variation with time for $\Delta\omega_{\text{step}} = 20\pi$ rad s^{-1} and $\phi = 0.1$ rad

To appreciate the significance of the error envelope, the phase error in Eq. (19) along with its envelope is plotted in Fig. 10, when the system is subject to a frequency step of 10 Hz and a phase jump of 0.1 rad. The values of natural frequency and damping ratio were chosen as 100π rad s^{-1} and 0.1, respectively. The phase error oscillations are damped from an initial $\phi_{t=0^+} = 0.1$ rad, indicating a phase error introduced at $t = 0$.

By symmetry in the positive and negative envelopes, the error band E at settling time t_0 is twice the positive envelope at t_0. i.e.

$$E = \frac{2e^{-\delta\omega_n t_0}}{\omega_n\sqrt{1-\delta^2}}\sqrt{c_1 - 2c_2\delta} \tag{21}$$

where

$$c_1 = {\Delta\omega_{\text{step}}}^2 + \phi^2{\omega_n}^2 \tag{22}$$

$$c_2 = \Delta\omega_{\text{step}}\phi\omega_n. \tag{23}$$

In order to optimize damping to achieve a minimum error band at settling time, for a given natural frequency, frequency step and phase jump, we differentiate E in Eq. (21) with respect to δ. i.e.

$$(-2\omega_n t_0 c_2)\delta^3 + (-c_2 + \omega_n t_0 c_1)\delta^2 + (c_1 + 2\omega_n t_0 c_2)\delta + (-c_2 - \omega_n t_0 c_1) = 0. \tag{24}$$

Having arrived at two equations (*viz.* Eqs. (21) and (24)) which give a vast insight into the design of filter parameters for better dynamic response, there can be several ways to approach them.

[1] This window is particularly chosen due to the known sluggishness in the response with $\delta > 1$, as can be shown analytically, but is beyond the scope of this paper.

3.1.1 Approach 1: Error Quantization

1. Define the frequency step $\Delta\omega_{\text{step}}$ and phase jump ϕ for which the system is to be designed
2. Specify the maximum error band E permitted at settling time t_0
3. Assume a value of damping ratio (say $\delta = 0.707$)
4. Calculate the natural frequency ω_n from Eq. (21)

Although this approach meets the error specification at time t_0, there may be other values of δ and ω_n which would meet the same requirement with faster transient response and better filter realizability. This is simply because the assumed value of δ is not optimized for the specified error.

3.1.2 Approach 2: Damping Optimization

1. Define the frequency step $\Delta\omega_{\text{step}}$ and phase jump ϕ for which the system is to be designed
2. Specify the desired settling time t_0
3. Assume a value of natural frequency (say $\omega_n = 100\pi$ rad s^{-1})
4. Calculate the damping ratio δ from Eq. (24)

Although this approach will yield an optimum δ for the given parameters, it may not meet the specified error criterion, since error is not quantized in this approach.

Equation (21) helps in quantizing the maximum error band at settling time, for a specified frequency step and phase jump. However, to arrive at this quantization, there can be numerous possible combinations of δ and ω_n satisfying Eq. (21), and trial and error is inevitable in fixing one and calculating the other. Moreover, hitting on the best pair of filter parameters (k_p, k_i) will be impossible even with numerous iterations. Equation (24), on the other hand, yields the most optimum damping ratio for the specified values of frequency step and phase jump, such that the error band is minimum at settling time, for the given parameters. Yet the error may not be contained to the user-specified limits, since Eq. (24) does not take error into account.

With further analysis and comparison of the above approaches, it would suffice to say that when Eq. (21) is used without Eq. (24), phase error is quantized to the limits, but at the cost of a non-optimum δ, which would translate to difficulty in practical implementation of the resulting loop filter and/or poorer dynamics. Also, when Eq. (24) is used without Eq. (21), damping is optimized, yet it may or may not meet the error specification, depending on the assumed value of ω_n. In other words, in both of the above approaches, one of the (δ, ω_n) pair is assumed to arrive at the other, and each has its own drawback.

It is here that we propose to treat Eqs. (21) and (24) as a self-consistent set of equations, which if solved iteratively, will yield a consistent solution of (δ, ω_n) for the specified E, t_0, $\Delta\omega_{\text{step}}$, and ϕ. We thus combine Approach 1 and 2 so as to eliminate their individual limitations of assumption. This novel approach guarantees that the solution confines the envelope of error at t_0 to the limits, and at the same time ensures that physically realizable (or practical) values of k_p and k_i are chosen, to achieve the desired dynamic performance optimally.

3.2 Solution of the Self-Consistent Equations

One of the challenges in this scheme, as may be visible on close observation of Eqs. (21) and (24), is that the solution of these equations is neither simple nor straightforward. While Eq. (24) is a cubic equation in δ, ω_n appears as the exponent in Eq. (21). Numerical techniques like the Newton–Raphson method can be used to solve for ω_n in Eq. (21).

In the context of solving Eq. (24), it is noteworthy to point that when $c_2 = 0$, then either $\phi = 0$ or $\Delta\omega_{\text{step}} = 0$. This is a specific case when the dynamic response of SRF PLL is to be tuned for any one of frequency step and phase jump, and not both. Thereby, Eq. (24) reduces to

$$\omega_n t_0 \delta^2 + \delta - \omega_n t_0 = 0 \tag{25}$$

which is quadratic in nature. On solving Eq. (25), the optimum damping ratio is given by

$$\delta = \frac{-1 + \sqrt{1 + 4{\omega_n}^2 {t_0}^2}}{2\omega_n t_0}. \tag{26}$$

However, when $c_2 \neq 0$, Eq. (24) cannot be reduced further. Cubic in nature, this equation may have either one real and two complex roots, or three real roots (of which two or three may even repeat). Clearly, further processing is needed to automate selection of the desired root from these cases. Moreover, in the context of optimized damping, it is crucial to qualify the presence of the optimum damping factor in the interval [0, 1]. Hence, it is imperative that a numerical scheme not be used in solving Eq. (24). Analytical methods such as Vieta's substitution or Cardan's method (published by Gerolamo Cardano in 1545) rely on the depressed cubic equation to yield the exact solution. Owing to its simple and elegant approach, we have adopted the Cardan's method to solve Eq. (24). Nevertheless, the proposed design methodology is not limited to its use, and any other analytical scheme can as well be employed for solving Eq. (24), provided the analysis on selecting the optimum damping factor is done for the respective scheme.

Table 2 Choice of optimum δ from Cardan's real roots

Possibility	Inference
1. All real roots fall in [0, 1]	This statement has been disproved through contradiction. It is impossible to have all real roots in [0, 1]
2. $E'(0) < 0$	
(i) $c_1 - 2c_2 \neq 0$	The error band has a negative slope at $\delta = 0$ and $E \to \infty$ as $\delta \to 1$. This leaves the possibility of only one stationary point in [0, 1]; Only one real root in [0, 1] of Cardan's real roots
(ii) $c_1 - 2c_2 = 0$	The error band has a negative slope at $\delta = 0$ and E is finite as $\delta \to 1$. Also, E is a decreasing function in [0, 1], thus eliminating the possibility of any stationary point in [0, 1]; No real root in [0, 1]. Choose optimum $\delta = 1$
3. $E'(0) > 0$	The error band has a positive slope at $\delta = 0$ and $E \to \infty$ as $\delta \to 1$. Also, E is an increasing function in [0, 1], thus eliminating the possibility of any stationary point in [0, 1]; No real root in [0, 1]. Choose optimum $\delta = 0$

Rewriting Eq. (24), we have

$$\delta^3 + \underbrace{\left(\frac{-c_2 + \omega_n t_0 c_1}{-2\omega_n t_0 c_2}\right)}_{l}\delta^2 + \underbrace{\left(\frac{c_1 + 2\omega_n t_0 c_2}{-2\omega_n t_0 c_2}\right)}_{m}\delta + \underbrace{\left(\frac{-c_2 - \omega_n t_0 c_1}{-2\omega_n t_0 c_2}\right)}_{n} = 0. \tag{27}$$

For Cardan simplification, we choose

$$p = m - \frac{l^2}{3} \tag{28}$$

$$q = \frac{2l^3}{27} - \frac{lm}{3} + n \tag{29}$$

where l, m and n are the respective coefficients in Eq. (27). Based on these coefficients, conclusions can be derived on the nature of the cubic roots. The inferences are listed here, a comprehensive analysis behind these inferences being presented in the Appendix.

If $\left(q^2 + \frac{4p^3}{27}\right) > 0$, then Eq. (27) has only one real root which is given by

$$\delta = \lambda - \frac{p}{3\lambda} - \frac{l}{3} \tag{30}$$

where

$$\lambda = \left[\frac{-q + \sqrt{q^2 + \frac{4p^3}{27}}}{2}\right]^{\frac{1}{3}}. \tag{31}$$

However, if $\left(q^2 + \frac{4p^3}{27}\right) \leq 0$, then all of the three roots of Eq. (27) are real, and the solution set is given by

$$\left\{\left[2r\cos\theta - \frac{l}{3}\right], \left[2r\cos\left(\theta + \frac{2\pi}{3}\right) - \frac{l}{3}\right], \left[2r\cos\left(\theta - \frac{2\pi}{3}\right) - \frac{l}{3}\right]\right\} \tag{32}$$

where

$$r = \left(\frac{-p}{3}\right)^{\frac{1}{2}} \tag{33}$$

$$\theta = \frac{1}{3}\tan^{-1}\frac{\sqrt{-\left(q^2 + \frac{4p^3}{27}\right)}}{-q}. \tag{34}$$

The real roots obtained in Eqs. (30) and (32) are basically solutions of the second equation [Eq. (24)] in the self-consistent pair, which indicate the optimum damping factors for the given conditions. However, we need a quantifying mechanism to select an optimum δ in the interval of interest, [0, 1], from these solutions. This post-solution analysis is detailed in the Appendix, and the conclusive inferences are listed in Table 2, which aid in selecting the optimum δ from Cardan's real roots.

3.3 The SCM Approach

Having solved the two self-consistent equations independently, yielding two values of δ and ω_n, each satisfying its own equation, the final objective is to find a unique (δ, ω_n) pair that satisfies both Eqs. (21) and (24). This approach is termed as the SCM, and is outlined in the following steps:

1. Assume a natural frequency to start with (say $\omega_n = 100\pi$ rad s^{-1})
2. With the available value of ω_n, solve Eq. (24) for δ using the Cardan's analytical scheme (dealt in Sect. 3.2)
3. With the value of δ obtained from Step 2, solve Eq. (21) for ω_n using the Newton–Raphson numerical scheme
4. Feed this value of ω_n obtained from Step 3 to Step 2, and repeat the cycle until a unique (δ, ω_n) pair is obtained, which would then satisfy both Eq. (21) and Eq. (24)

As a result, we observe that this approach combines two methodologies, namely error quantization and damping opti-

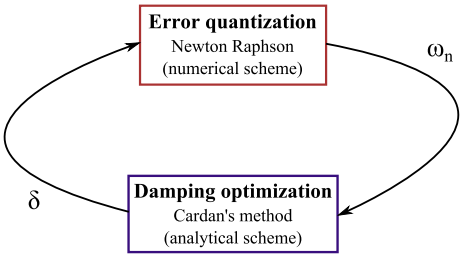

Fig. 11 The SCM

mization, into one entity called the SCM, to yield a consistent solution that is unique and the most optimum. Symbolically, this approach may be expressed as in Fig. 11. Once the design converges on a unique (δ, ω_n) pair, the filter parameters *viz.*, proportional gain k_p, integral gain k_i, and time constant τ, can be found as

$$k_p = \frac{2\delta\omega_n}{E_m} \tag{35}$$

$$k_i = \frac{{\omega_n}^2}{E_m} \tag{36}$$

$$\tau = \frac{k_p}{k_i} = \frac{2\delta}{\omega_n}. \tag{37}$$

To study the convergence of this procedure, different initial values of ω_n are chosen in Step 1 and the SCM is iterated until the solutions of δ and ω_n converge to their 6th and 3rd decimal places, respectively. With initial values of ω_n chosen close to the convergent value, as few as two iterations are required to attain the desired accuracy. Even with initial values far from the convergent ω_n, the procedure converges in five or less iterations. Since fewer iterations are needed to yield a useful approximation, the rate of convergence is said to be high.

4 Conclusions

Having established the theory of the SCM with a direct and mathematically correct procedure in Part 1, Part 2 of this paper analyses the proposed scheme under a range of grid imperfections. Extensive comparisons with the traditional Wiener technique help in appreciating the performance improvement when applied to three of the existing SRF-based 3-phase PLLs from literature.

Appendix

A Analysis of Cardan's Roots Through Analytic Means

A.1 *Cardan's Solution to the Cubic Equation in δ*

Consider the general form of a cubic equation

$$ax^3 + bx^2 + cx + d = 0. \tag{38}$$

When $a \neq 0$, Eq. (38) can be re-written as

$$x^3 + lx^2 + mx + n = 0 \tag{39}$$

where $l = b/a$, $m = c/a$ and $n = d/a$. Substituting $y = x + l/3$, Eq. (39) becomes

$$y^3 + py + q = 0 \tag{40}$$

where p and q are the Cardan simplifiers given in Eqs. (28) and (29), respectively. Let $y = u + v$. i.e.

$$y^3 - 3uvy - (u^3 + v^3) = 0. \tag{41}$$

On comparing the coefficients of Eqs. (40) and (41), we get

$$uv = -\frac{p}{3} \tag{42}$$

$$u^3 + v^3 = -q. \tag{43}$$

Solving Eqs. (42) and (43) yields

$$u^3 = \frac{-q + \sqrt{q^2 + \frac{4p^3}{27}}}{2}. \tag{44}$$

The roots of Eq. (44) are given by

$$u = \left\{\lambda\ ,\ \lambda\omega\ ,\ \lambda\omega^2\right\} \tag{45}$$

where λ is as shown in Eq. (31) and

$$\omega = e^{j\frac{2\pi}{3}} = \frac{-1 + \sqrt{3}j}{2} \tag{46}$$

$$\omega^2 = e^{-j\frac{2\pi}{3}} = \frac{-1 - \sqrt{3}j}{2}. \tag{47}$$

On back substitution of the values of u from Eq. (45), we consequently obtain the values of x, which satisfy Eq. (39) as

$$x = \left\{\left[\lambda - \frac{p}{3\lambda} - \frac{l}{3}\right]\ ,\ \left[\lambda\omega - \frac{p}{3\lambda\omega} - \frac{l}{3}\right]\ ,\ \left[\lambda\omega^2 - \frac{p}{3\lambda\omega^2} - \frac{l}{3}\right]\right\}. \tag{48}$$

Thus, the roots of the cubic equation in Eq. (39) are found by Cardan's technique.

A.2 *Nature of the Roots*

Of the three roots found using Cardan's method, either one root may be real and the other two imaginary, or all three

roots may be real. To arrive at the condition for three real roots, a calculus-based approach is followed. Let

$$f(y) = y^3 + py + q. \tag{49}$$

As can be inferred from inspection, the cubic function is unbound. i.e. $f(y) \in (-\infty, +\infty)$. Also, for three roots to be real, $f(y)$ curve should intersect the $f(y) = 0$ axis thrice (or at least twice, in case two of the real roots are equal). The stationary points of $f(y)$ are given by

$$y = \pm\sqrt{\frac{-p}{3}} = \pm\, y_0 \quad \text{(say)} \tag{50}$$

and the local extrema *viz.*, $f(-y_0) = f_{\max}$ and $f(+y_0) = f_{\min}$ are as shown in Fig. 12.

For the existence of three real roots, the stationary points of $f(y)$ should be real and the product $f_{\max}.f_{\min}$ should be either negative or zero. i.e.

$$p < 0 \tag{51}$$

$$f_{\max}.f_{\min} \leq 0. \tag{52}$$

On simplification, Eq. (52) becomes

$$q^2 + \frac{4p^3}{27} \leq 0. \tag{53}$$

Conditions in Eqs. (51) and (53) are thus necessary for the existence of three real roots. However, Eq. (51) is already included in Eq. (53). Therefore, Eq. (53) becomes the necessary and sufficient condition for the three roots to be real.

A.3 *Choice of Optimum* δ *in* [0, 1]

Having arrived at the solutions to the cubic equation, it is crucial to qualify the presence of a real root in the region of interest; i.e. the optimum δ in [0, 1]. Following are the possibilities that would require further analysis in selecting the optimum δ:

- All of the three real roots from Eq. (32) may lie in [0, 1]
- Two of the three real roots from Eq. (32) may lie in [0, 1]
- None of the three real roots from Eq. (32) may lie in [0, 1]
- The only real root from Eq. (30) may not lie in [0, 1]

A systematic approach is followed to conclude on the valid cases analytically.

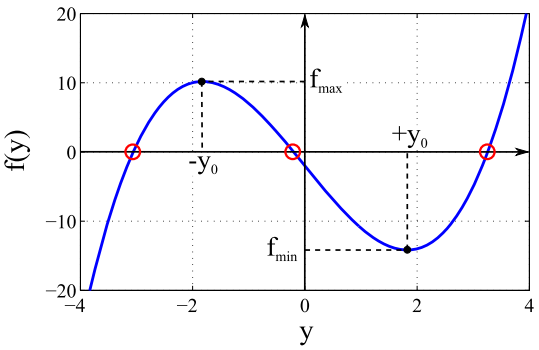

Fig. 12 A cubic function $f(y)$ with three real roots, two stationary points $(-y_0, +y_0)$ and the respective local extrema $(f_{\max}, f_{\min})$ marked

Case 1: Three Real Roots Lie in [0, 1]

This possibility can be overruled through contradiction. Let the three real roots *viz.*, δ_1, δ_2 and δ_3 lie in [0, 1]. Then the sum and product of roots are given by

$$\delta_1 + \delta_2 + \delta_3 = -l \tag{54}$$

$$\delta_1.\delta_2.\delta_3 = -n. \tag{55}$$

Since δ_1, δ_2 and $\delta_3 \in [0, 1]$,

$$\delta_1 + \delta_2 + \delta_3 > 0 \quad \text{and} \quad \delta_1.\delta_2.\delta_3 > 0. \tag{56}$$

This implies

$$l + n < 0. \tag{57}$$

But from Eq. (24), we have

$$l + n = \frac{-c_2 + \omega_n t_0 c_1}{-2\omega_n t_0 c_2} + \frac{-c_2 - \omega_n t_0 c_1}{-2\omega_n t_0 c_2} \tag{58}$$

$$= \frac{1}{\omega_n t_0} \tag{59}$$

which is always positive. Clearly, Eqs. (57) and (59) are an inconsistency, and the initial assumption is incorrect. Thus, it is impossible for the three real roots of Eq. (32) to lie in [0, 1].

Case 2: Two Real Roots Lie in [0, 1]

Two aspects *viz.*, slope of the phase error band at $\delta = 0$ and the limiting value of phase error band as $\delta \to 1$, are used to conclude that two real roots from Eq. (32) cannot lie in [0, 1].

1. The slope of the error expression in Eq. (21) at $\delta = 0$ is given by

$$E'(\delta)\Big|_{\delta=0} = E'(0) = \frac{2}{\omega_n\sqrt{c_1}}\Big\{-(c_2 + \omega_n t_0 c_1)\Big\} \tag{60}$$

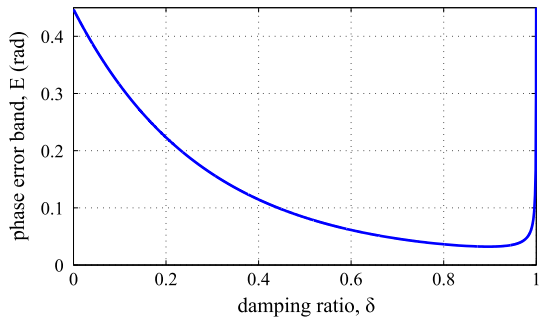

Fig. 13 Variation of error band with damping ratio, for $\Delta\omega_{\text{step}} = 20\pi$ rad s^{-1}, $\phi = 0.1$ rad, $\omega_n = 100\pi$ rad s^{-1} and $t_0 = 0.01$ s (One real root in [0, 1])

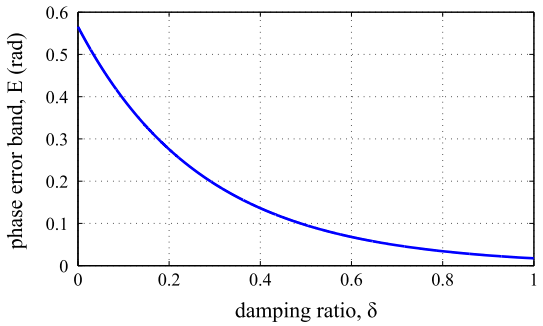

Fig. 14 Variation of error band with damping ratio, for $\Delta\omega_{\text{step}} = 20\pi$ rad s^{-1}, $\phi = 0.2$ rad, $\omega_n = 100\pi$ rad s^{-1} and $t_0 = 0.01$ s (No real root in [0, 1] - First corner case)

2. The limiting value of the phase error band as $\delta \to 1$ is given by

$$E(\delta)\Big|_{\delta\to 1} = \lim_{\delta\to 1} \frac{2e^{-\delta\omega_n t_0}}{\omega_n\sqrt{1-\delta^2}}\sqrt{c_1 - 2c_2\delta} \tag{61}$$

If $c_2+\omega_n t_0 c_1 > 0$, then from Eq. (60), $E'(0) < 0$. Physically, this means that the rate of change of $E(\delta)$ is negative as δ increases from zero. From Eq. (61), $E \to \infty$ as $\delta \to 1$, provided $c_1 - 2c_2 \neq 0$.

Since the error band initially decreases from $\delta = 0$ and eventually approaches infinity as $\delta \to 1$, there can be either one or three stationary points in [0, 1] which satisfy this nature. However, since the possibility of three real roots in [0, 1] is eliminated previously, the only possibility is the existence of one real root in [0, 1], which can either be from Eq. (30) or Eq. (32). For one such specific case, the variation of error band is shown in Fig. 13.

Case 3: No Real Root Lies in [0, 1]

There can be two corner cases when none of Cardan's real roots from Eqs. (30) or (32) lie in [0, 1].

1. First corner case: When $c_2+\omega_n t_0 c_1 > 0$ and $c_1-2c_2 = 0$, the error band has an initial negative slope ($E'(0) < 0$) and the limiting value of E is finite as $\delta \to 1$. In other words, the error band initially decreases from $\delta = 0$, and has a finite value at $\delta = 1$. This leaves us with the possibility of either zero or two stationary points in [0, 1]. Substituting $c_1 = 2c_2$ in Eq. (21), the error band becomes

$$E = \frac{2e^{-\delta\omega_n t_0}}{\omega_n\sqrt{1+\delta}}\sqrt{2c_2} \tag{62}$$

which is a continually decreasing function with δ. This eliminates the possibility of two stationary points in [0, 1]. Hence, for this case, there is no stationary point in [0, 1], and the minimum error band occurs at $\delta = 1$, as shown in Fig. 14.
The optimum δ for this corner case is chosen as $\delta = 1$.

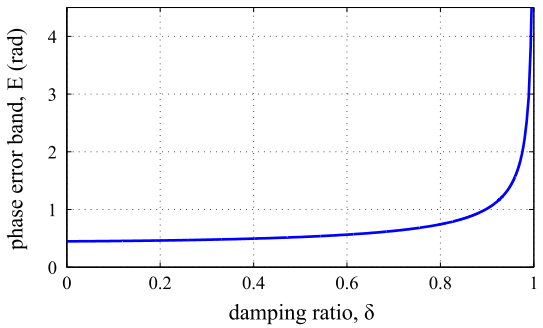

Fig. 15 Variation of error band with damping ratio, for $\Delta\omega_{\text{step}} = 20\pi$ rad s^{-1}, $\phi = -0.1$ rad, $\omega_n = 100\pi$ rad s^{-1} and $t_0 = 0.001$ s (No real root in [0, 1] - Second corner case)

2. Second corner case: When $c_2 + \omega_n t_0 c_1 < 0$, the error band has an initial positive slope ($E'(0) > 0$). Also, since c_1 is always positive from Eq. (22), $c_2 + \omega_n t_0 c_1 < 0$ implies that c_2 is negative; i.e. $c_1 - 2c_2 \neq 0$. Thus, $E \to \infty$ as $\delta \to 1$, from Eq. (61). Since the error band initially increases from $\delta = 0$, and approaches infinity as $\delta \to 1$, there can be either zero or two stationary points in [0, 1]. To eliminate the possibility of two stationary points of $E(\delta)$ in [0, 1], consider $E'(\delta)$ given by

$$E'(\delta) = \frac{2e^{-\delta\omega_n t_0}}{\omega_n\left(1-\delta^2\right)^{\frac{3}{2}}\sqrt{c_1 - 2c_2\delta}}\, f(\delta) \tag{63}$$

where

$$f(\delta) = (-2\omega_n t_0 c_2)\delta^3 + (-c_2 + \omega_n t_0 c_1)\delta^2 + (c_1 + 2\omega_n t_0 c_2)\delta + (-c_2 - \omega_n t_0 c_1) \tag{64}$$

From Eq. (64), the following are implied, specifically for this corner case:

- $f(0) > 0$
- $f(1) > 0$
- $f'(0) > 0$
- $f'(1) > 0$

- Neither of the two stationary points of $f(\delta)$ lie in [0, 1] Thus, $f(\delta)$ is always increasing in [0, 1]. Since $f(\delta)$ has no roots in [0, 1], there cannot be two stationary points of $E(\delta)$ in [0, 1]. The only other possibility is that $E(\delta)$ has no stationary points and is always increasing with δ in [0, 1], as shown in Fig. 15. Since the minimum error band occurs at $\delta = 0$, the optimum δ for this case is chosen as $\delta = 0$.

The various possibilities are explored and the invalid cases are eliminated. The consolidated inferences in choosing the optimum δ on solving the cubic Eq. (24) by Cardan's method are listed in Table 2.

References

Blackburn, J. L. (1993). *Symmetrical components for power systems engineering* (1st ed.). Boca Raton: CRC Press.

Bollen, M. H. J. (1996). Fast assessment methods for voltage sags in distribution systems. *IEEE Transaction on Industry Application*, *32*(6), 1414–1423.

Chung, S. K. (2000). A phase tracking system for three phase utility interface inverters. *IEEE Transactions on Power Electronics*, *15*(3), 431–438.

da Silva, C. H., Pereira, R. R., da Silva, L. E. B., Lambert-Torres, G., Bose, B. K., & Ahn, S. U. (2010). A digital PLL scheme for three-phase system using modified synchronous reference frame. *IEEE Transactions on Industrial Electronics*, *57*(11), 3814–3821.

Gardner, F. M. (2005). *Phaselock Techniques* (3rd ed.). New Jersey: John Wiley & Sons Inc.

Golestan, S., Monfared, M., Freijedo, F. D., & Guerrero, J. M. (2012). Design and tuning of a modified power-based PLL for single-phase grid-connected power conditioning systems. *IEEE Transactions on Power Electronics*, *27*(8), 3639–3650.

González-Espín, F., Figueres, E., & Garcerá, G. (2012). An adaptive synchronous-reference-frame phase-locked loop for power quality improvement in a polluted utility grid. *IEEE Transactions on Industrial Electronics*, *59*(6), 2718–2731.

Gulez, K. (2008). Neural network based switching control of AC-AC converter with DC-AC inverter for voltage sags, harmonics and EMI reduction using hybrid filter topology. *Simulation Modelling Practice and Theory*, *16*(6), 597–612.

Guo, X., Wu, W., & Chen, Z. (2011). Multiple-complex coefficient-filter-based phase-locked loop and synchronization technique for three-phase grid-interfaced converters in distributed utility networks. *IEEE Transactions on Industrial Electronics*, *58*(4), 1194–1204.

Karimi-Ghartemani, M., & Iravani, M. R. (2004). A method for synchronization of power electronic converters in polluted and variable-frequency environments. *IEEE Transactions on Power Systems*, *19*(3), 1263–1270.

Kaura, V., & Blasko, V. (1997). Operation of a phase locked loop system under distorted utility conditions. *IEEE Transactions on Industry Applications*, *33*(1), 58–63.

Kesler, M., & Ozdemir, E. (2011). Synchronous-reference-frame-based control method for UPQC under unbalanced and distorted load conditions. *IEEE Transactions on Industrial Electronics*, *58*(9), 3967–3975.

Krause, P. C., Wasynczuk, O., & Sudhoff, S. D. (2002). *Analysis of electric machinery and drive systems*. New Jersey: IEEE Press.

Kulkarni, A., & John, V. (2013). Analysis of bandwidth - unit vector distortion trade off in PLL during abnormal grid conditions. *IEEE Transactions on Industrial Electronics*, *60*(12), 5820–5829.

Lee, K. J., Lee, J. P., Shin, D., Yoo, D. W., & Kim, H. J. (2014). A novel grid synchronization PLL method based on adaptive low-pass notch filter for grid-connected PCS. *IEEE Transactions on Industrial Electronics*, *61*(1), 292–301.

Liccardo, F., Marino, P., & Raimondo, G. (2011). Robust and fast three-phase PLL tracking system. *IEEE Transactions on Industrial Electronics*, *58*(1), 221–231.

Rodríguez, P., Pou, J., Bergas, J., Candela, I., Burgos, R., Boroyevich, D. (2005) Double synchronous reference frame PLL for power converters control. In: Proc. 36th IEEE PESC, pp 1415–1421.

Rodríguez, P., Teodorescu, R., Candela, I., Timbus, A., Liserre, M., Blaabjerg, F. (2006) New positive-sequence voltage detector for grid synchronization of power converters under faulty grid conditions. In: Proc. 37th IEEE PESC, pp 1–7.

Rodríguez, P., Pou, J., Bergas, J., Candela, J. I., Burgos, R. P., & Boroyevich, D. (2007). Decoupled double synchronous reference frame PLL for power converters control. *IEEE Transactions on Power Electronics*, *22*(2), 584–592.

Wang, L., Jiang, Q., Hong, L., Zhang, C., & Wei, Y. (2013). A novel phase-locked loop based on frequency detector and initial phase angle detector. *IEEE Transactions on Power Electronics*, *28*(10), 4538–4549.

Weidenbrug, R., Dawson, F. P., & Bonert, R. (1993). New synchronization method for thyristor power converters to weak AC-systems. *IEEE Transactions on Industrial Electronics*, *40*(5), 505–511.